TECHNICAL NOTE

Rapid prototyping of noncontact microwave microfluidic devices for sensing applications

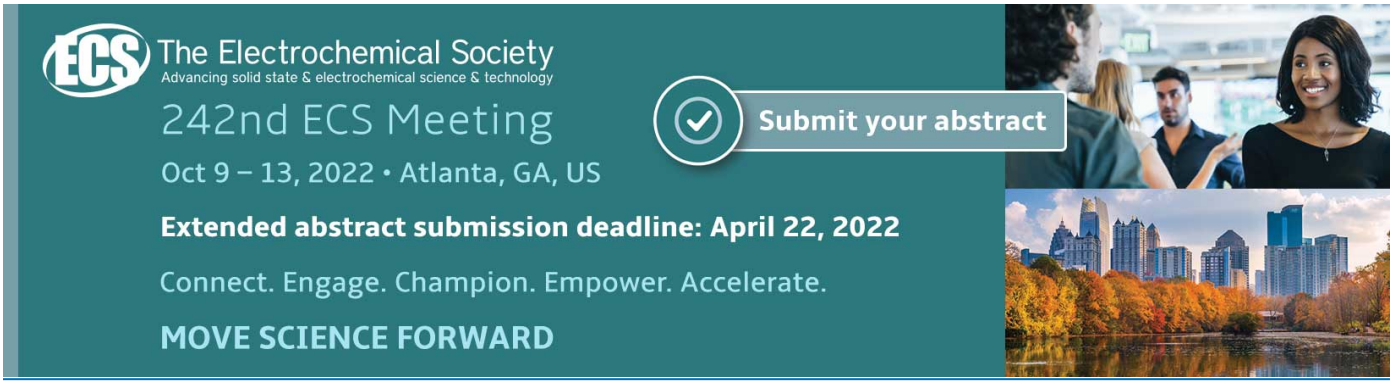

IOP Publishing Journal of Micromechanics and Microengineering
J. Micromech. Microeng. **31** (2021) 097001 (8pp) https://doi.org/10.1088/1361-6439/ac1a86

Technical Note

Rapid prototyping of noncontact microwave microfluidic devices for sensing applications

Berk Camli[1], Oguz Kaan Erden[1], Ozan Furkan Sezgen[1], Zeliha Cansu Canbek Ozdil[2,*], Sema Dumanli[1], Ali Emre Pusane[1], Arda Deniz Yalcinkaya[1] and Tuna Tugcu[2]

[1] Department of Electrical and Electronics Engineering, Bogazici University, Istanbul 34342, Turkey
[2] Computer Engineering Department, Bogazici University, 34342 Istanbul, Turkey

E-mail: cansu.canbek@boun.edu.tr

Received 12 March 2021, revised 24 July 2021
Accepted for publication 4 August 2021
Published 18 August 2021

Abstract

Microfluidics is an innovative technological platform with a vast potential to streamline processes in biology, chemistry, and biomedical fields. Microfluidic integrated biosensors attract much attention due to extreme miniaturization, low sample consumption, and increased homogeneity in mixing conditions, leading to enhanced sensitivity. Nowadays, many researchers focus on inexpensive and flexible laser production of polymer-based microfluidic devices for sensing applications due to their ease of production and rapid processing benefits. In this article, we present some key factors for the simple and rapid production of microfluidic components of the microwave sensor by using the CO_2 laser ablation technique. The technique does not require any cleanroom or complex laboratory setups and provides short fabrication times for prototyping. It is observed that, at high laser power (30 W) and low scan speed (125 cm s^{-1}), both the channel depth and the surface roughness increase greatly as opposed to channel waviness. It is also demonstrated that heat treatment is a viable method to reduce the channel roughness with a trade of channel depth. In the second section, prepared channels are bonded onto the split ring resonators (SRRs) fabricated using polymethyl methacrylate as a substrate. Power reflection measurements from SRR are performed using a continuous flow system that injects 100 mM glucose solutions into the channels. Change of dielectric constant due to glucose loading generates a meaningful resonance frequency shift, showing a possible use scenario of the device as a biosensor.

Keywords: microfluidics, laser engraving, roughness, split ring resonator, lab on chip sensor

(Some figures may appear in colour only in the online journal)

1. Introduction

Microfluidic technology is a novel platform dealing with behavior, precise control, and manipulation of fluids confined to a small, typically sub-millimeter, scale [1]. The technology dates to the 1950s, to the development of inkjet printers. Afterward, the principle of using silicon-based micromachining of microvalves and micropumps was advanced in the 1960s [2].

Recently, many efforts have been spent on microelectromechanical integrated microfluidics systems, especially for biomedical sensing [3]. These modern technology devices provide users high sensitivity and reliability while offering other advantages such as high-quality factor, reagent minimization, real-time measurement possibility due to short

* Author to whom any correspondence should be addressed.

diffusion times, reduced process cost, non-contact measurement possibility, etc [3, 4].

Following the integration of microfluidic devices with electromechanical systems to realize point-of-care testing, the need for complex laboratory setup and experienced personnel is no longer required to perform sensing. Additionally, due to the large surface-to-volume ratio gained in micro-scale (compared to macro-scale), higher sensitivity and sensing performance can be achieved [5, 6]. In view of these advantages, integration of microfluidics with other sensing systems creates new possibilities for the future of biosensing applications.

Production of microfluidic devices initially commenced with the patterning of silicon-based polymers by a complex manufacturing technique called lithography [7]. The method is based on local exposure of a radiation-sensitive polymer to form crosslinks to obtain minimized features on the desired substrate [8, 9]. After that, the patterned design is utilized as a mold and can be used to produce silicon-based microfluidic devices. The method is very costly and time-consuming, and the availability of cleanroom facilities is a must. Considering the contamination in many microfluidic applications, single-use devices are desired, making lithography not the first choice of production. Apart from lithographic patterning, many other production techniques have been developed for micropatterning of microfluidic channels, such as hot embossing [10], injection molding [11], casting, 3D printing [12], and laser ablation [13].

All these fabrication techniques are considered relatively complex and expensive due to high-cost equipment requirements. Laser ablation is an alternative method of micro-production based on removing the material from the surface by using focused electromagnetic radiation [14]. Different types of laser systems can be used for micro-production, such as ultra-violet (UV) [15–18] or continuous infrared (IR) lasers. In the case of a UV laser, a high energy light is used for the targeted breakdown of the material in very short pulses, whereas for IR laser systems, a computer-controlled CO_2 laser set-up is used for the ablation of the designed pattern on the surface of the desired substrate under continuous IR radiation, [19–22]. Channel dimensions are controlled by laser power, scanning speed, and the distance between the substrate surface and the focal plane of the laser beam in both systems [14]. Although both techniques have been used for microfabrication, UV lasers are not commonly preferred due to low repeatability [23].

In the case of IR lasers, designed channels are etched on the surface of the substrate without the need for any mold or photomask and can easily be used with a wide variety of low-cost polymers. Channel dimensions can be controlled by laser power, scanning speed, and the distance between the substrate surface and the focal plane of the laser beam.

Polymethyl methacrylate (PMMA) is one of the most distinguished substrates that has been used in laser engraving due to its thermal stability, low diffusivity, low cost, and strong chemical resistance. Additionally, the material provides high gas impermeability and mechanical robustness, making it a frequently used material in microfluidic chip fabrication [24, 25]. Although the material properties can easily vary depending on the purity, it also offers to create single-use devices in bulk due to its low cost.

Table 1. A summary of the previous works performed on the reduction of surface roughness in PMMA based microfluidic devices obtained by CO_2 laser engraving technique.

Author	Surface enhancement	Roughness (R_a)
Cheng *et al* [30]	Thermal annealing	2.04 nm
Wang *et al* [28]	Wet chemical surface etching	10 nm
Huang *et al* [27]	Pre-eating	100.86 nm
Mohammed *et al* [31]	Multi-pass	1.5–2.5 μm
Han *et al* [32]	Preheating	5 μm

Even though CO_2 laser engraving is a quite promising technique for micro-production, it also brings some disadvantages that need to be solved, such as high manufacturing defects, surface roughness, and low control over microchannel depth [8, 26]. Low surface roughness is the desired parameter, since roughness has a direct impact on the flow and transportation phenomena. Additionally, the high surface roughness may block the microchannels by accumulating residual deposits due to burrs and gouges along the channel and may affect the flow regime locally. Hence, improving the surface roughness and smoothness of microchannel surfaces has become an important issue. While tremendous work has been done to reduce the surface roughness by performing pre-and post-processing techniques, such as tempering the substrate before ablation [27], surface etching by a variety of solvents [26, 28], two pass micromachining [29], there is still a long way for improvement. Table 1 summarizes the achieved surface roughnesses in various works.

In this work, we present a novel prototyping method to produce a microfluidics integrated electromagnetic resonator lab-on-chip system for sensing applications with low surface roughness. Initially, we report a full characterization of PMMA microfluidic channel surfaces, prepared by fast prototyping with CO_2 laser ablation technique by modifying two major parameters in laser during micromachining: laser speed and power. We have employed a faithful approach to determine the optimum input parameters for laser machining by combining focus stacking and profilometer analysis. The second part of the study is dedicated to the production of the microwave resonator incorporating a microfluidic lab-on-chip sensor, prepared by using optimized process parameters described in the first section. As-produced channels are bonded with metamaterial-inspired split-ring-resonator (SRR) structures printed using silver (Ag) ink by a precision dispensing system. Finally, preliminary results, along with the measurement setup, are presented.

2. Sensor fabrication

2.1. Microfluidic channel design and production

Commercially available PMMA sheets, with the size of 2 mm × 200 mm × 300 mm, were used as microfluidic

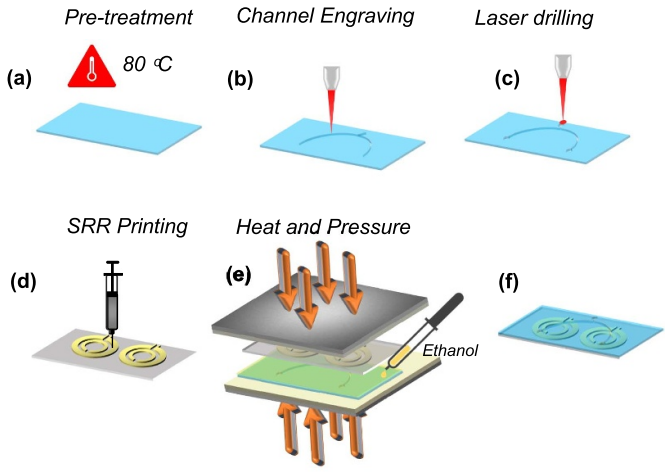

Figure 1. Schematic representation of micro engraving process.

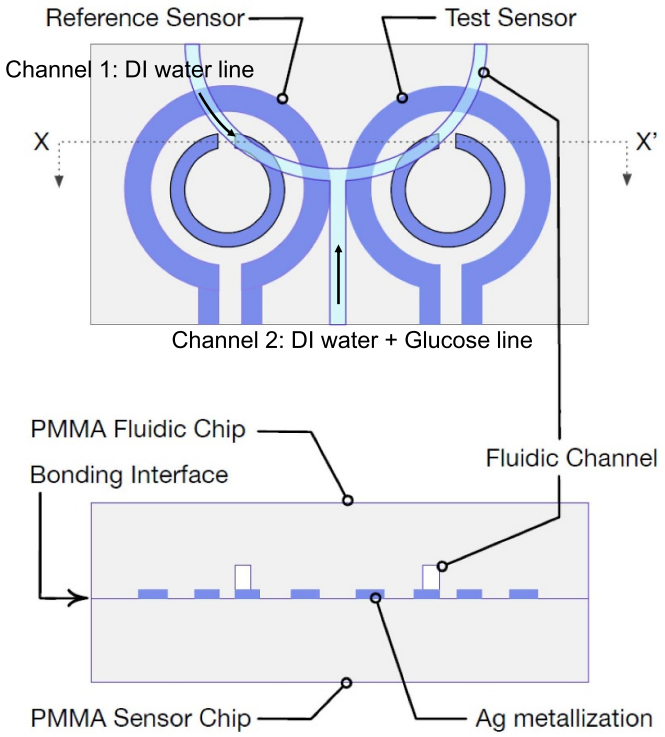

Figure 2. (Top) Geometric structure of the SRR design, loop antenna, microfluidic channel. (Bottom) Cross-sectional view of the sensor structure across the X–X' line marked on the top figure.

chip material. For profile and topography analysis, rectangular 10 mm × 0.6 mm microfluidic channels were drawn in AutoCad Software, and the outputs were exported to VersaLaser Software. For micro-production, Versalaser VL-200 CO_2 laser, at a wavelength of 10.6 μm, was used at variable laser power (3–30 W), and scan speed (125–500 cm s^{-1}) settings. Schematic descriptions of the process and the experimental setup used during engraving experiments are represented in figure 1. All experiments include a single pass of the laser beam fixed at a constant focal height of 100 mm from the top of the surface. With the beam size on the focused spot as 31 μm, the maximum surface power density is calculated as 2.4×10^6 W cm^{-2}.

To analyze the effects of temperature on the engraved channels, a separate set of PMMA samples were exposed to heat (80 °C) for 3–5 min before the engraving procedure. To ensure that thermal treatment on the PMMA surface was successfully performed, a contact angle analysis was done on both thermally treated and untreated PMMA surfaces by the sessile drop method. Typically, 10 μl milli-Q water is placed on the surface of the substrate, and eight sets of images of the droplet have been collected. The experiments have been repeated 3 times per set. Collected images have been analyzed using the ImageJ software with the Contact Angle plugin. Preheated samples were engraved at different scanning speeds and laser power levels, as in the case of untreated samples. These were then compared with the samples fabricated without any heat treatment.

The channel profile data was obtained by using a Dektak XT stylus profiler from Bruker instruments. Both transverse and longitudinal directions were used for the profilometer scan. Recorded surface profile data were then processed with Gaussian regression filters built in the Vision 64 software (Bruker instruments) to be separated into its waviness and roughness components. Roughness was then quantified using the arithmetical mean deviation definition of roughness, which was denoted as Ra. Longitudinal roughness was calculated over a longer segment (2 mm on average) compared to the transverse roughness case, where a flatter, shorter (50 μm in average) segment was used. Segment lengths used in the calculation of transverse roughness for preheated samples were even shorter (10 μm on average) since the overall channel profile approximates a bell curve, where relatively flat segments in transverse direction were harder to observe.

Additional analyses of microchannels were done by different imaging methods for a qualitative comparison of the channel profiles. The depth of field analysis (DOF) is performed initially by merging a stack of images acquired at different focus heights using an optical microscope. In this way, we obtained an entirely focused composite image which is then used to create a 3D surface plot of the ablated section by the ImageJ plugin 'Interactive 3D surface plot'. Scanning electron microscopy (SEM) was also employed for imaging engraved channels. SEM images were obtained by using Philips XL30 environmental SEM at 5 kV.

2.2. SRR and loop antenna design and production

SRR with various shapes is the most frequently used structure in which the sensing principle is based on electromagnetic interaction of the analyte with the resonator [33–35]. These sensors are distinguished by their simple design, ease of fabrication, low cost, high sensitivity, quality factor, contactless operation, and reliable measurement capability [36]. Due to its ability to concentrate electric fields in a single sensitive area at its gap, the basic circular SRR structure shown in figure 2 is

used in this work. The microchannel is designed to pass around the inner gap of the SRR, where the electric field distribution has higher sensitivity to obtain at the desired level of frequency shift, [37].

The ring resonator has an inner ring radius of R, the inductive component L, and capacitance C. The main component capacitance has two main contributions from gap capacitance C_{gap} and surface capacitance C_{sur} as shown in equation (1) [38]:

$$C = C_{gap} + C_{sur}. \tag{1}$$

The resonance frequency f_0 of the SRR can be engineered based on equation (2),

$$f_0 = \frac{1}{2\Pi\sqrt{LC}}. \tag{2}$$

In this work, the SRRs are coupled to individual loop antennas surrounding them. With the loop antennas, measurements can be done by using a single port per single resonator. To maintain a high Q value in a simple structure, conductive silver ink, with a conductivity value of 1250 S cm^{-1}, and PMMA substrate with lower dielectric loss are used for printing. Based on this principle, an SRR with f_0 at 1.525 GHz was designed to be fabricated on a 76 × 52 mm^2 PMMA substrate. Voltera V-One is used for the precision printing of the reference and the test SRR's by depositing conductive ink on the substrate with high precision and thermally curing the ink with its integrated heater.

Bonding of microchannel and resonator was realized using the solvent binding technique with a manual sublimation heat press. The technique involves applying a thin layer of ethanol (70% v/v) onto both PMMA layers that will be bonded. Afterward, the layers are pressed between the hot press plates with an additional copper plate for 250 s at 105 °C.

2.3. Measurement set-up

The measurement set-up is given in figure 3. The reflection coefficients of reference and test SRRs, S11 and S22, respectively, were used for analysis. S11 and S22 represent the measure of reflected power at each port and are frequency dependent. The power sent to the port will be received by the SRR structure, minimizing the reflection at its resonant frequency. Hence, S11 and S22 can be used to track the resonant frequency of the SRRs. Measurements were conducted using a Vector Network Analyzer (Rohde & Schwarz ZNL VNA). Before analyte loading, the reflection spectra for SRR containing deionized (DI) water is recorded. Next, 100 mM glucose solution is introduced from the middle channel (channel 2) by using a micro syringe pump operating at a flow rate of 100 μl min^{-1}, while DI water is flowing through channel 1 at flow rate of 100 μl min^{-1} . The silicone tubing of 3 × 4 mm (I.D × O.D) is used for the connection. The measurements were repeated five times for each case.

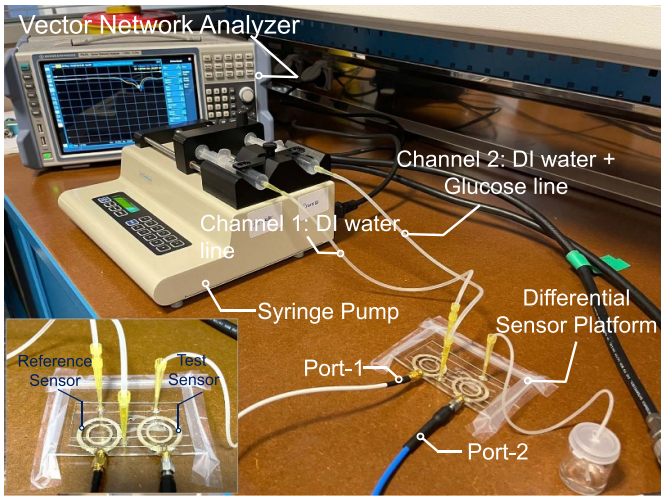

Figure 3. Measurement set-up.

3. Results and discussion

3.1. Microfluidic channel characterization

Initial tests include changing the two main parameters in the CO_2 laser, power (3–30 W) and scanning speed (125–500 cm s^{-1}) to ascertain the impact of the laser parameters on surface topography. 3D surface plots, obtained from DOF analysis of microscopy images, are given in figure 4. At high laser power (24–30 W) and low scan speed (125 cm s^{-1}), the macro-scale waviness of the channels is quite low in comparison to the low laser power (6–18 W) and high scan speed (500 cm s^{-1}) cases.

The channels ablated at 30 W and 125 cm s^{-1} scan speed bears smooth and wider profiles, whereas the channels ablated at 6 W and 500 cm s^{-1} yields shallower and wavy surfaces. The reason for observing such a difference in the surface topography can be explained by the fact that the PMMA is not a thermally stable material and will decompose to its monomer around 220 °C under laser irradiation [39]. This process yields the combustion of methyl methacrylate (MMA) into smaller gaseous products. At constant laser power (30 W), it is possible that increased local temperature permits enough time for molten PMMA to vaporize in the form of MMA for low scan speed (125 cm s^{-1}), whereas for high scan speeds (500 cm s^{-1}), the ablated MMA re-solidifies in the scanned location [30].

Based on the data obtained from profilometer readings, surface roughness, R_a, was calculated both for longitudinal and transverse directions at different laser power and speed values. The results presented in figures 5(a) and (b) indicate that the surface roughness tends to increase with higher laser power and lower scan speed for both longitudinal and transverse directions as opposed to waviness. This is attributed to the transfer of the induced heat to the material surface, which is quite effective throughout the melting and removal of the substance during the channel engraving process. Globally, the longitudinal roughness values are between 0.3 μm and 4.3 μm, whereas the transverse roughness values have a range around 0.06 μm–1 μm.

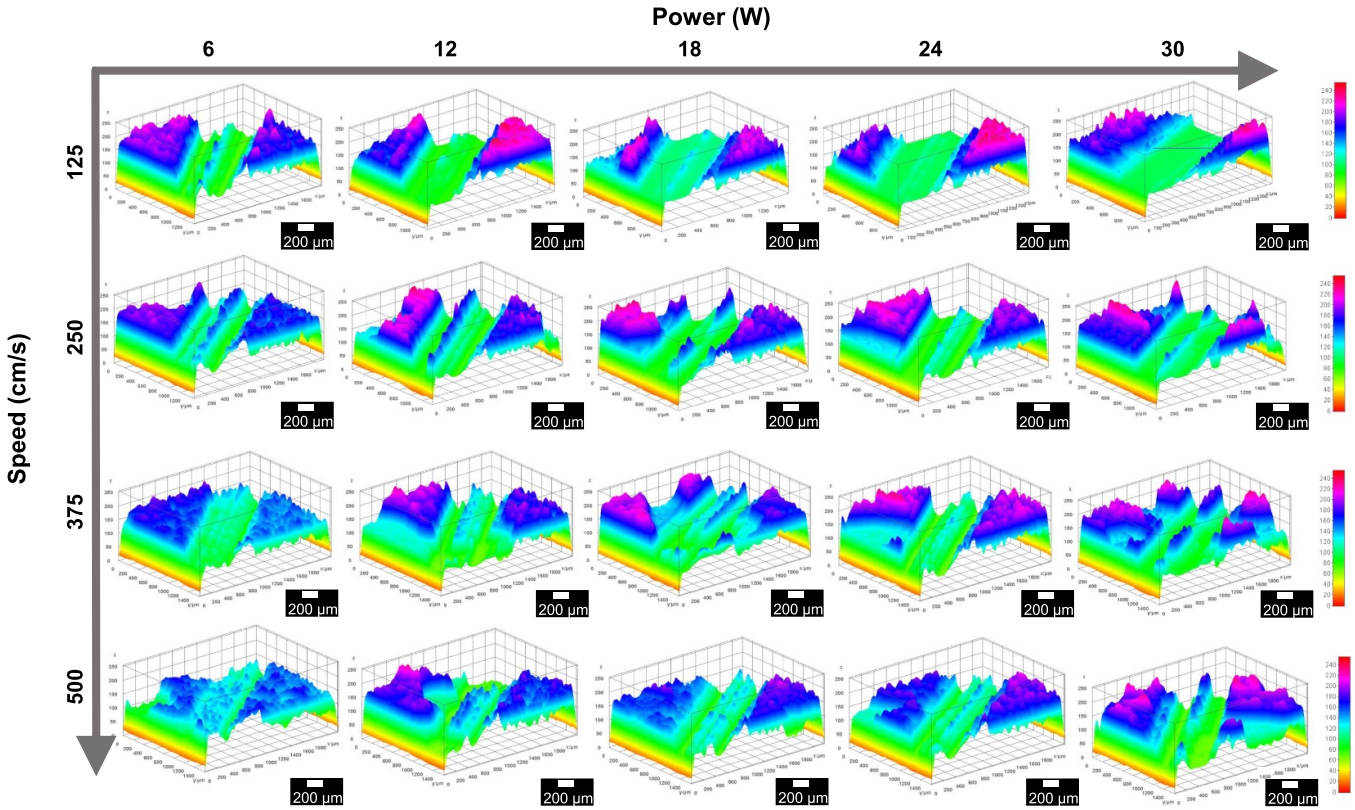

Figure 4. Three-dimensional surface images of the engraved PMMA at different laser power (3–30 W) and scan speed (125–500 cm s^{-1}) values.

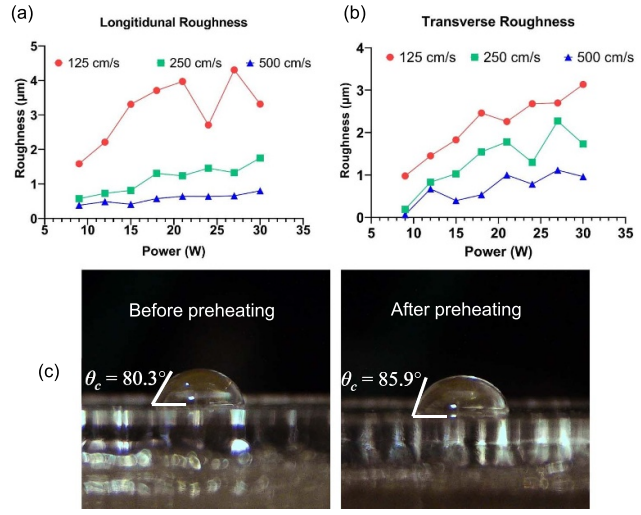

Figure 5. (Top) Surface roughness of microchannels in (a) longitudinal and (b) transverse directions at varying laser power and scan speed levels. (Bottom) Contact angle of water droplets (left) before preheating (right) after preheating.

The contact angle measurements performed on samples subjected to heat treatment demonstrate a change in the surface property of the PMMA. As shown in figure 5(c), the contact angle of the milli-Q water droplet with the PMMA surface increases to 85.9° ± 0.4° after the heat treatment process from its original value of 80.3 ± 0.3°. Such an increase agrees with the previous studies and confirms that the preheating modifies the chemical composition of the PMMA surface and increases wettability [40].

The effects of preheating on both longitudinal and transverse surface roughness values are presented in table 2 for two different power (18–30 W) and scan speed (125–500 cm s^{-1}) levels. The longitudinal surface roughness of the PMMA before the heat treatment is 1.8738 μm for scan speed of 125 cm s^{-1} at 18 W. It is observed that, after the heat treatment, the roughness decreases to 0.9651 μm. The heat treatment significantly reduces the surface roughness for both directions throughout the channel. The reason for such a decrease is mainly due to the thermal decomposition of the polymer under heat. SEM images of PMMA channels prepared without any treatment and with preheating are shown in figures 6(a) and (b). Mainly, the microchannel surface, prepared by untreated PMMA, bears a large number of trapped microbubbles at the interface (figure 6(a)) due to rapid temperature increase during ablation, causing the pronounced roughness [27]. Preheating the PMMA layer (figure 6(b)) close to the glass transition temperature where the phase transition between the solid and gas phase starts ensures that the bubbles escape from the transition layer easily during ablation. R_a values for heat-treated channels still follow an increasing pattern with increased laser power and decreased laser speed values, similar to those without preheating. The reduction is more prominent in the transverse direction.

Following a similar type of analysis performed initially for surface roughness, we employed the same parametric data alteration (laser power, scan speed) to correlate the channel

Table 2. Effect of heat treatment on the surface roughness in longitudinal and transverse directions of microchannels fabricated using laser power of 18 W and 30 W with the scan speed of 125 cm s^{-1} and 500 cm s^{-1}.

	Longitudinal roughness (μm)				Transverse roughness (μm)			
	No pretreatment		Pretreatment		No pretreatment		Pretreatment	
	$s = 125$ cm s^{-1}	$s = 500$ cm s^{-1}	$s = 125$ cm s^{-1}	$s = 500$ cm s^{-1}	$s = 125$ cm s^{-1}	$s = 500$ cm s^{-1}	$s = 125$ cm s^{-1}	$s = 500$ cm s^{-1}
$P = 18$ W	1.873	0.175	0.965	0.009	0.398	0.240	0.003	0.003
$P = 30$ W	2.866	0.269	1.773	0.067	0.893	0.348	0.017	0.067

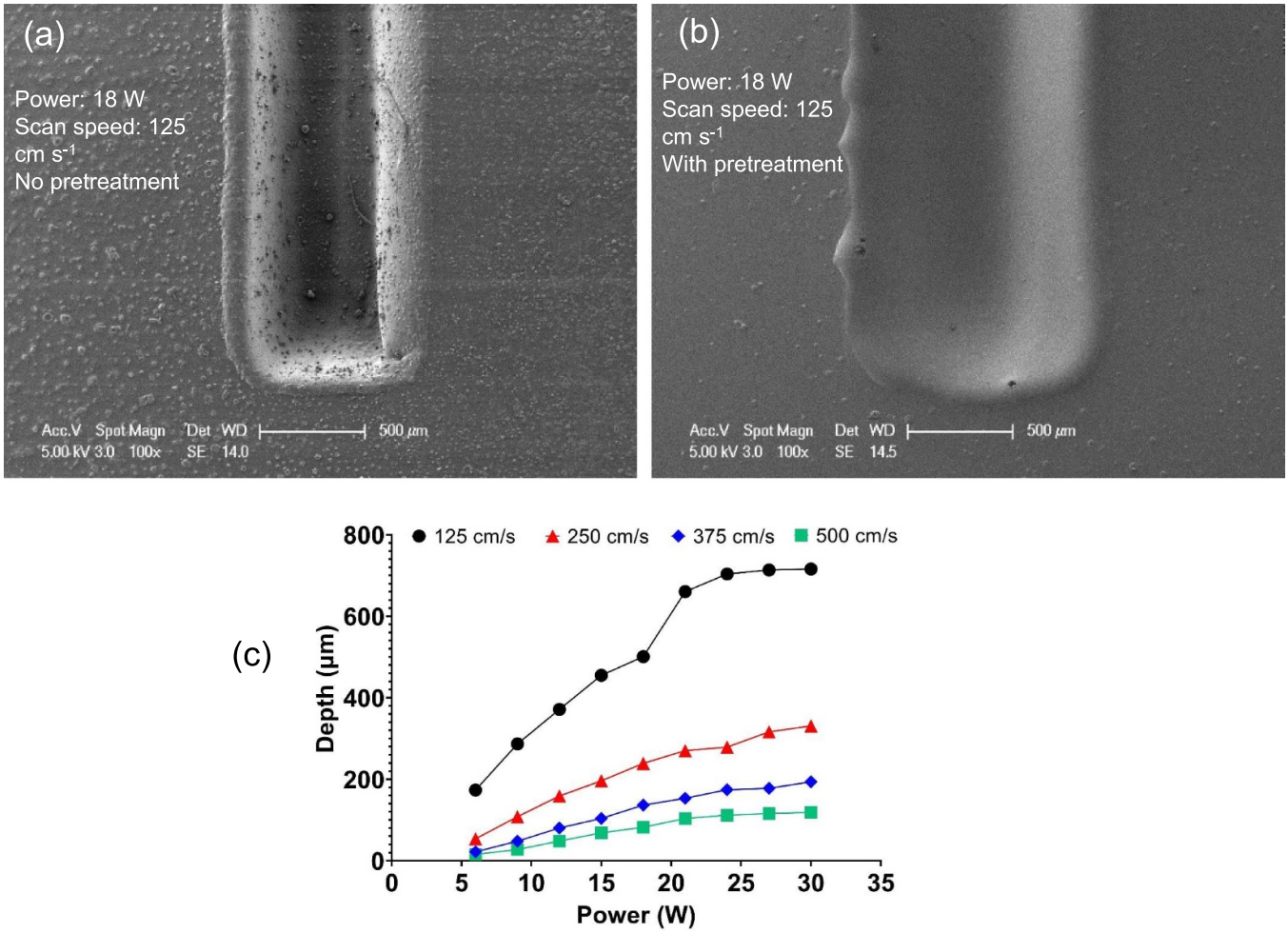

Figure 6. SEM images of the l microchannels at a laser power of 18 W and speed of 125 cm s^{-1} (a) no pretreatment (b) preheated to 80 °C. (c) Effect of laser power and surface pre-treatment on the channel depth of engraved microchannels at varying fabrication parameters.

depth with these parameters. The results are summarized in figure 6(c). Analysis indicates a direct correlation between the channel depth, laser power, and scan speed. With high laser power (30 W) and low scan speed (125 cm s^{-1}), it is probable that the beam can easily penetrate the polymer and ablate deeper microchannels to generate a depth of 768 μm. For the preheated samples, channel depths were found to be consistently lower than their non-preheated counterparts (table 3).

3.2. SRR and loop antenna measurements

In microwave sensing experiments, the microchannels are prepared by using laser power of 18 W and scan speed of 500 cm s^{-1} since these parameters yield low surface roughness and deep channel profile. In the next step, a 100 mM glucose solution is introduced to the microchannel. Five subsequent measurements were taken. The averages of the measurements and the absolute difference between the measure and reference readings are shown in figure 7. Reference and test sensors reveal different nominal resonance frequencies stemming from the fabrication tolerances in pattern transfer and printing processes.

Differential measurements are obtained by measuring the reflection parameters for reference and test sensors as a function of frequency. Figure 7 shows results for nominal and loaded states of the microchannels. For the sensing

Table 3. Effect of heat treatment on depth of microchannels fabricated using scan speed of 125 cm s^{-1} and 500 cm s^{-1} with laser power of 6,18, 30 W.

	Depth (μm)			
	No pretreatment		Pretreatment	
	$s = 125$ cm s^{-1}	$s = 500$ cm s^{-1}	$s = 125$ cm s^{-1}	$s = 500$ cm s^{-1}
$P = 6$ W	175.773	7.664	86.274	2.437
$P = 18$ W	517.029	72.224	366.164	21.953
$P = 30$ W	768.613	107.506	490.421	35.462

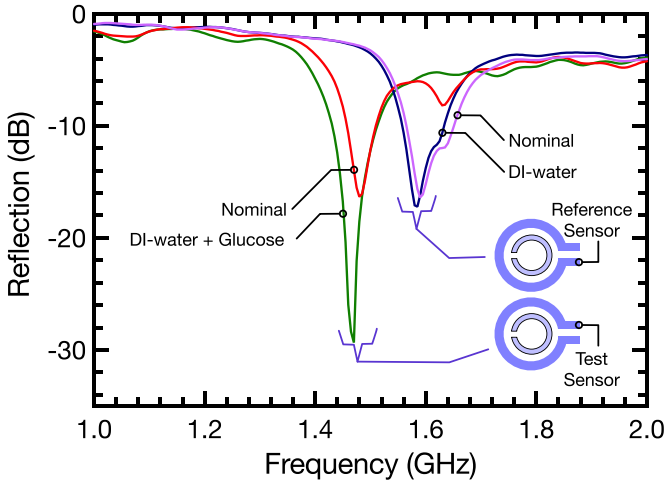

Figure 7. Differential reflection measurements for the reference and the test sensors.

experiment, the reference device is loaded with DI water as the test device is loaded with DI water and 100 mM glucose solution. As expected, the test device exhibits a larger resonance frequency shift (1%) in comparison to the reference device (0.3%). Change of dielectric constant on the test device due to glucose loading generates a meaningful resonance frequency shift, demonstrating a possible use scenario of the device as a biosensor.

4. Conclusion

In this work, a simple approach to microwave incorporating microfluidic-based sensor design was studied. The approach lends flexibility and simplicity to the fact that any 2D design can be realized in an automated engraving procedure by using PMMA as a substrate. These designs can be incorporated into electromagnetic resonator structures for sensing applications. Moreover, the method allows rapid prototyping of the device. A trade-off between the channel depth and surface roughness has been observed. The depth and roughness increase with increased laser power and decreased scanning speed. A saturation behavior in channel depth is observed as the laser power is increased beyond a certain point at low scanning speed values, which is not observed in the surface roughness behavior. Roughness values evaluated in both transverse and longitudinal directions are found in the same order of magnitude.

The proposed system has been utilized to demonstrate a preliminary glucose sensing platform. SRR platform generated promising results. The nominal value of the reference sensor is measured as 1.595 GHz, and it shifts to 1.592 GHz, which gives a 0.3% change in the resonance frequency, whereas the nominal value of the test sensor is measured as 1.485 GHz, and it shifts to 1.475 GHz, which corresponds to 1% frequency change. Thus, a meaningful resonance frequency shift has been observed as the dielectric constant changed due to glucose loading.

Data availability statement

All data that support the findings of this study are included within the article (and any supplementary files).

Acknowledgments

This work was supported in part by the Turkish Directorate of Strategy and Budget under the TAM Project Number DPT2007K120610, the Scientific and Technical Research Council of Turkey (TUBITAK) under Grant 119E190, and Bogazici University Research Fund under Project Number 18202.

ORCID iD

Zeliha Cansu Canbek Ozdil https://orcid.org/0000-0001-9420-567X

References

[1] Whitesides G M 2006 The origins and the future of microfluidics *Nature* **442** 368–73
[2] Nguyen Nam-Trung and Wereley Steven 2006 *Fundamentals and Applications of Microfluidics* Second Edition (Boston : *Artech House*) (Artech)
[3] Ashraf M W, Tayyaba S and Afzulpurkar N 2011 Micro electromechanical systems (MEMS) based microfluidic devices for biomedical applications *Int. J. Mol. Sci.* **12** 3648–704
[4] Zarifi M H, Sadabadi H, Hejazi S H, Daneshmand M and Sanati-Nezhad A 2018 Noncontact and nonintrusive microwave-microfluidic flow sensor for energy and biomedical engineering *Sci. Rep.* **8** 139
[5] Luka G, Ahmadi A, Najjaran H, Alocilja E, DeRosa M, Wolthers K, Malki A, Aziz H, Althani A and Hoorfar M

2015 Microfluidics integrated biosensors: a leading technology towards lab-on-a-chip and sensing applications *Sensors* **15** 30011–31
[6] Ma Y-D, Li K-H, Chen Y-H, Lee Y-M, Chou S-T, Lai -Y-Y, Huang P-C, Ma H-P and Lee G-B 2019 A sample-to-answer, portable platform for rapid detection of pathogens with a smartphone interface *Lab Chip* **19** 3804–14
[7] Xia Y and Whitesides G M 1998 Soft lithography *Angew. Chem., Int. Ed.* **37** 550–75
[8] Gale K B, Jafek A, Lambert C, Goenner B, Moghimifam H, Nze U and Kamarapu S 2018 A review of current methods in microfluidic device fabrication and future commercialization prospects *Inventions* **3** 60
[9] Madou M J 2002 *Fundamentals of Microfabrication: The Science of Miniaturization* 2nd edn (Boca Raton, FL: CRC Press) (Accessed 26 October 2020)
[10] Heckele M and Schomburg W K 2003 Review on micro molding of thermoplastic polymers *J. Micromech. Microeng.* **14** R1–R14
[11] Giboz J, Copponnex T and Mélé P 2007 Microinjection molding of thermoplastic polymers: a review *J. Micromech. Microeng.* **17** R96–R109
[12] McDonald J C, Chabinyc M L, Metallo S J, Anderson J R, Stroock A D and Whitesides G M 2002 Prototyping of microfluidic devices in poly(dimethylsiloxane) using solid-object printing *Anal. Chem.* **74** 1537–45
[13] Mohammed M I, Quayle K, Alexander R, Doeven E, Nai R, Haswell S J, Kouzani A Z and Gibson I 2015 Improved manufacturing quality and bonding of laser machined microfluidic systems *Proc. Technol.* **20** 219–24
[14] Benton M, Hossan M R, Konari P R and Gamagedara S 2019 Effect of process parameters and material properties on laser micromachining of microchannels *Micromachines* **10** 123
[15] Gomez D, Goenaga I, Lizuain I and Ozaita M 2005 Femtosecond laser ablation for microfluidics *Opt. Eng.* **44** 1–8
[16] Juodėnas M, Tamulevičius T, Ulčinas O and Tamulevičius S 2017 Implementation of an optimized microfluidic mixer in alumina employing femtosecond laser ablation *J. Micromech. Microeng.* **28** 015013
[17] Queste S, Salut R, Clatot S, Rauch J-Y and Khan Malek C G 2010 Manufacture of microfluidic glass chips by deep plasma etching, femtosecond laser ablation, and anodic bonding *Microsyst. Technol.* **16** 1485–93
[18] Suriano R, Kuznetsov A, Eaton S M, Kiyan R, Cerullo G, Osellame R, Chichkov B N, Levi M and Turri S 2011 Femtosecond laser ablation of polymeric substrates for the fabrication of microfluidic channels *Appl. Surf. Sci.* **257** 6243–50
[19] Klank H, Kutter J P and Geschke O 2002 CO_2-laser micromachining and back-end processing for rapid production of PMMA-based microfluidic systems *Lab Chip* **2** 242–6
[20] Wang S-C, Lee C-Y and Chen H-P 2006 Thermoplastic microchannel fabrication using carbon dioxide laser ablation *J. Chromatogr.* A **1111** 252–7
[21] Hong T-F, Ju W-J, Wu M-C, Tai C-H, Tsai C-H and Fu L-M 2010 Rapid prototyping of PMMA microfluidic chips utilizing a CO_2 laser *Microfluid. Nanofluidics* **9** 1125–33
[22] Hou -H-H, Wang Y-N, Chang C-L, Yang R-J and Fu L-M 2011 Rapid glucose concentration detection utilizing disposable integrated microfluidic chip *Microfluid Nanofluidics* **11** 479–87
[23] Khan Malek C G 2006 Laser processing for bio-microfluidics applications (part II) *Anal. Bioanal. Chem.* **385** 1362–9
[24] Shaegh S A M *et al* 2018 Rapid prototyping of whole-thermoplastic microfluidics with built-in microvalves using laser ablation and thermal fusion bonding *Sens. Actuators* B **255** 100–9
[25] Hou X, Zhang Y S, Santiago G T-D, Alvarez M M, Ribas J, Jonas S J, Weiss P S, Andrews A M, Aizenberg J and Khademhosseini A 2017 Interplay between materials and microfluidics *Nat. Rev. Mater.* **2** 17016
[26] Addae-Mensah K A, Wang Z, Parsa H, Chin S Y, Laksanasopin T and Sia S K 2010 Fundamentals of microfluidics devices *Microfluidic Devices in Nanotechnology* (New York: Wiley) pp 1–38
[27] Huang Y, Liu S, Yang W and Yu C 2010 Surface roughness analysis and improvement of PMMA-based microfluidic chip chambers by CO_2 laser cutting *Appl. Surf. Sci.* **256** 1675–8
[28] Wang Z K, Zheng H Y, Lim R Y H, Wang Z F and Lam Y C 2011 Improving surface smoothness of laser-fabricated microchannels for microfluidic application *J. Micromech. Microeng.* **21** 095008
[29] Prakash S and Kumar S 2015 Profile and depth prediction in single-pass and two-pass CO_2 laser microchanneling processes *J. Micromech. Microeng.* **25** 035010
[30] Cheng J-Y, Wei C-W, Hsu K-H and Young T-H 2004 Direct-write laser micromachining and universal surface modification of PMMA for device development *Sens. Actuators* B **99** 186–96
[31] Mohammed M I, Zainal Alam M N H, Kouzani A and Gibson I 2016 Fabrication of microfluidic devices: improvement of surface quality of CO_2 laser machined poly(methylmethacrylate) polymer *J. Micromech. Microeng.* **27** 015021
[32] Han X, Liu X, Tian L, Zhang H and Mao Z-G 2015 A non-photolithography fabrication for a microfluidic chip based on PMMA polymer *Machines* **3** 107–22
[33] Jaruwongrungsee K, Waiwijit U, Withayachumnankul W, Maturos T, Phokaratkul D, Tuantranont A, Wlodarski W, Martucci A and Wisitsoraat A 2015 Microfluidic-based split-ring-resonator sensor for real-time and label-free biosensing *Proc. Eng.* **120** 163–6
[34] Vélez P, Muñoz-Enano J, Grenier K, Mata-Contreras J, Dubuc D and Martín F 2019 Split ring resonator-based microwave fluidic sensors for electrolyte concentration measurements *IEEE Sens. J.* **19** 2562–9
[35] Camli B and Yalcinkaya A D 2021 Resonant type RF glucose biosensors *Reference Module in Biomedical Sciences* (Amsterdam: Elsevier) (https://doi.org/10.1016/B978-0-12-822548-6.00011-X)
[36] Prakash D and Gupta N 2021 Applications of metamaterial sensors: a review *Int. J. Microw. Wirel. Technol.* 1–15
[37] Camli B, Altinagac E, Kizil H, Torun H, Dundar G and Yalcinkaya A D 2020 Gold-on-glass microwave split-ring resonators with PDMS microchannels for differential measurement in microfluidic sensing *Biomicrofluidics* **14** 054102
[38] Nilsson J W and Riedel S A 1996 *Electric Circuits* 5th edn ed J W Nilsson and S A Riedel (Reading, MA: Addison-Wesley)
[39] Zeng W R, Li S F and Chow W K 2002 Review on chemical reactions of burning poly(methyl methacrylate) PMMA *J. Fire Sci.* **20** 401–33
[40] Matellan C and Del Río Hernández A E 2018 Cost-effective rapid prototyping and assembly of poly(methyl methacrylate) microfluidic devices *Sci. Rep.* **8** 6971